Mechanism of reverse current increase of vertical-type diamond Schottky diodes

T. Teraji,[1,a)] A. Fiori,[1,2] N. Kiritani,[3] S. Tanimoto,[3,4] E. Gheeraert,[2] and Y. Koide[1]
[1]*National Institute for Materials Science, 1-1 Namiki, Tsukuba, Ibaraki 305-0044, Japan*
[2]*Université Grenoble Alpes, CNRS, Grenoble INP, Institut Néel, F38000 Grenoble, France*
[3]*Nissan Motor Co., Ltd., 1, Natsushima, Yokosuka, Kanagawa 237-8523, Japan*
[4]*Nissan Arc Ltd., 1, Natsushima, Yokosuka, Kanagawa 237-0061, Japan*

(Received 5 July 2017; accepted 3 September 2017; published online 4 October 2017)

Current transport at *p*-diamond Schottky contacts under reverse bias operation was investigated. Reverse current transport modes of several types were observed depending on the bias voltage range: thermionic emission (TE) associated with the image force barrier lowering was dominant in the lower voltage range of <50 V, whereas thermionic-field emission (TFE) mechanism governed transport in the higher voltage range. The Schottky barrier height ϕ_b estimated from the reverse characteristics was lower than that obtained from the forward characteristic by more than 0.4 eV, which indicates that the low Schottky barrier height ϕ_b^{low} area localized in the patch shape at the diamond Schottky contact. This Schottky contact inhomogeneity was found to increase the reverse current effectively even though the ϕ_b^{low} area is smaller because the reverse current in TE mode flows preferentially through ϕ_b^{low} patches. The current transport mode changed from TE to TFE when the maximum electric field was >1 MV cm^{-1}, which indicates that a strong electric field concentration exists at the Schottky electrode fringe. When the high reverse voltage was biased, a sudden current increase occurred, followed by a permanent increase of reverse current, indicating that mid-gap defects were formed at the interface. These results indicate that reverse current and electric-field breakdown have different origins. *Published by AIP Publishing.*
[http://dx.doi.org/10.1063/1.4994570]

I. INTRODUCTION

During the past decade, diamond Schottky barrier diodes (SBD) have been studied intensively to realize high-performance rectifiers providing both high-voltage resistance in reverse operation and low on-resistance in forward operation, which is difficult to achieve using common semiconductor materials. Several interesting results have been reported to date from using diamond.[1,2] At the same time, difficulties that must be resolved before practical applications have been pointed out. An important issue among those is the low reproducibility of diode performance, especially related to the markedly high reverse current level and its large variation at a high bias voltage.[3,4] This strong reverse current makes diamond SBDs less attractive when considering power device applications because diamond is a semiconductor that is expected to have low reverse current properties at a high reverse voltage compared to other commonly used semiconductors. Dislocation in diamond crystal is an important factor increasing its reverse current. Imperfect fabrication of Schottky contacts is another factor inducing reverse current.[5,6] For the realization of power-device-grade diamond SBDs, we specifically examined establishment of a process for fabricating stable Schottky contacts with better reproducibility.

In the case of silicon SBDs, a silicide interlayer is formed intentionally to stabilize the rectification properties.[5,6] Although one can adapt the same scenario for diamond SBDs, in reality, carbide formation by the post-annealing of metal deposition degrades the rectification properties, resulting in the formation of ohmic contact for diamond.[7] A possible mechanism for this degradation is the outer diffusion of carbon atoms from the diamond surface, accompanied by vacancy-type defect formation at an elevated temperature because carbide phase is likely to be formed.[7] As a consequence, the leakage current flowing through these defects increases considerably.

To form an abrupt carbide/diamond Schottky contact while suppressing interface carbide formation, we deposited carbide-preformed metal directly on the diamond surface as Schottky electrodes. Tungsten carbide WC was chosen as Schottky electrode metal for this study because it has good mechanical strength and inertness for natural oxidation. These are important factors for the practical applications. In fact, high-temperature stability of WC/diamond interfaces has been reported.[8] Moreover, unique photo-response properties of WC/*p*-diamond SBDs have been investigated.[9] In this article, current transport at the WC/*p*-diamond interface is discussed, particularly addressing the reverse characteristics under high-voltage operation.

II. EXPERIMENTAL

To simplify the analysis of electric properties, a vertical SBD structure was employed. p^--diamond thin films were deposited homoepitaxially on a highly boron-doped (100) diamond single crystal substrate using home-made microwave plasma-assisted chemical vapor deposition (MPCVD).

[a)]E-mail: TERAJI.Tokuyuki@nims.go.jp

The respective thicknesses and boron atomic concentrations of p^+ substrates were 500 μm and 10^{20} cm^{-3}. The source gas used was a mixture of high-purity H_2 (9N-grade) and CH_4 (6N5-grade). Although the boron source gas was not injected into the reactor during diamond growth, boron was unintentionally incorporated in the homoepitaxial layer because the MPCVD reactor used here is commonly used for boron doping. A certain amount of boron can be supplied from the reaction chamber. Actually, the grown diamond film showed *p*-type conductivity. Secondary ion mass spectrometry (SIMS) using O_2^+ as probing ions instead of Cs^- to lower the minimum detection level to boron was used to provide an impurity depth profile. The acceleration voltage of probing ions was 15 kV. Figure 1 presents a typical SIMS depth profile of the p^-/p^+ stacking structure. The film thicknesses and boron atomic concentrations of p^--diamond layer were estimated, respectively, as 0.49 μm and approximately 2×10^{15} cm^{-3}. The thinner the p^- layer, the larger the maximum electric field that is applicable by a common current measurement system. However, it is difficult to evaluate acceptor concentration of such a lower doping level and a thinner layer which is located on the highly conductive substrate using Hall measurement or cathodoluminescence. To eliminate graphitic components before metal electrode deposition, the diamond surface was wet-chemically oxidized using a boiling acid mixture of nitric acid and sulfuric acid at approx. 200 °C.

The SBD structure is presented schematically in Fig. 2 along with the top view image of the sample. WC Schottky contacts were formed on the p^- homoepitaxial diamond surface, although Ti electrodes capped with WC were deposited on the whole area of the bottom p^+ diamond substrate surface as ohmic electrodes. To eliminate graphitic components before metal electrode deposition, the diamond surface was wet-chemically oxidized using a boiling acid mixture of nitric acid and sulfuric acid at approx. 200 °C. The fabrication process sequence is the following: first, a Ti/WC layer was deposited on the chemically oxidized p^+-diamond surface, followed by 600 °C annealing in an Ar environment using a

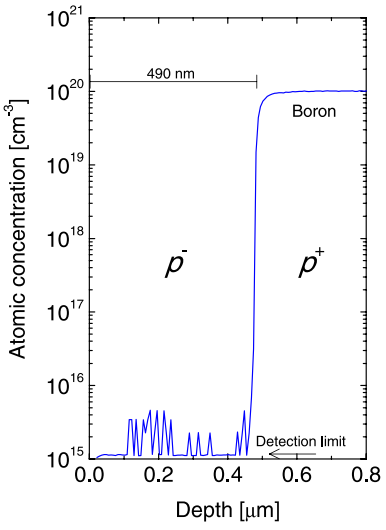

FIG. 1. Depth profile of boron in diamond p^-/p^+ stacking layer evaluated using secondary ion mass spectrometry.

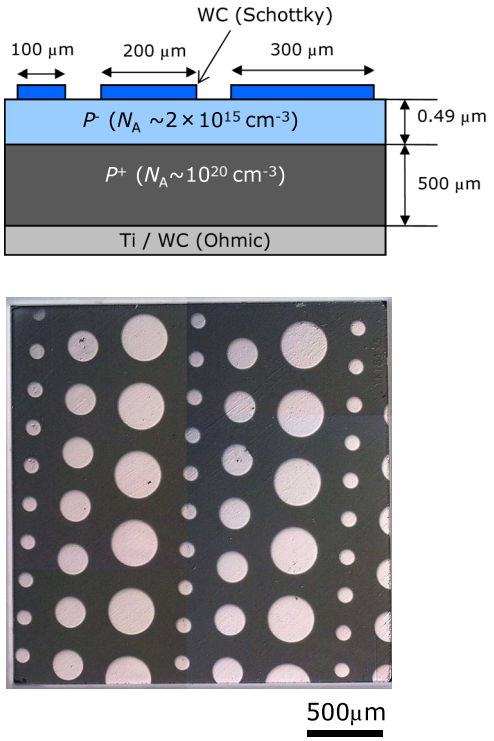

FIG. 2. Schematic cross section of the SBD structure and top view of the sample.

quartz-tube furnace to form ohmic contacts. Then, the WC Schottky contacts were formed on the oxidized p^--diamond surface. All metal deposition was done using a magnetron sputtering system with base pressure of approx. 10^{-7} Pa. The diamond sample was not intentionally heated during metal deposition. The sputtering target metal was a WC plate with a composition ratio of (1:1). Electrode patterns were fabricated using the metal shadow mask. The WC Schottky electrode diameters were 100, 200, or 300 μm. The deposition rate, which was monitored by quartz crystal microbalance during deposition, was approx. 0.1 nm s^{-1} under optimal conditions.[10] The actual electrode thickness was checked using an ultraviolet laser microscope with repeat accuracy of 14 nm and depth display of 1 nm. The electrode thickness was approx. 20 nm, which was sufficient to obtain a continuous film. The composition ratio of the deposited WC layer is almost equal to that of the target metal.[10] Electrical measurements were taken at room temperature (299 ± 1 K) using two tungsten microprobes with 25 μm radius of curvature. A picoammeter/voltage source (6487; Keithley Instruments, Inc.) was used for current–voltage measurements. To eliminate surface discharge effects, the diamond surface was covered with insulating liquid (Fluorinert FC-40; 3M, Inc.).

III. RESULTS

A. Forward characteristics

Figure 3 presents typical forward current–density voltage (J_F–V) characteristics of WC SBD with an electrode diameter of 100 μm. Here, the current density was defined as the forward current divided by the Schottky electrode area. Schottky barrier height ϕ_b of the WC Schottky electrodes

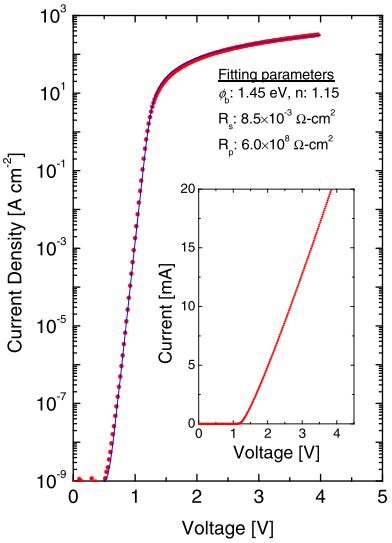

FIG. 3. Typical forward current density–voltage characteristic of WC SBDs with different electrode diameters. The inset shows the corresponding current–voltage characteristic.

was estimated from the fitting of J_F-V forward characteristics using the thermionic emission (TE) model of the SBD theory considering the ideality factor n, series areal resistivity R_s, and parallel areal resistivity R_p. The fitting curve is described as[5,6,11]

$$J_F = A^*T^2 \exp\left(\frac{-q\phi_b}{kT}\right) \times \left[\exp\left(\frac{-q(V - J_F \times R_s)}{nkT}\right) - 1\right] + \frac{V - J_F \times R_s}{R_p}, \quad (1)$$

where A^* signifies the Richardson constant, T stands for the absolute temperature, ϕ_b represents the Schottky barrier height, k denotes the Boltzmann constant, and q is the elemental charge. A^* of 90 A cm^{-2}K^{-2} and T of 300 K were used for this fitting. The fitted values were, respectively, ϕ_b=1.45 eV, n = 1.15, R_s = 8.5 mΩ cm^2, and R_p = 0.6 GΩ cm^2. Compared to the lateral SBD structure, R_s of the vertical SBD was less than four orders of magnitude.[12] R_p of both vertical and lateral structures were comparable. Smaller R_s of the vertical structure originates mainly from the decrease of parasitic resistance components, which is dominated by the series resistance of p^--type diamond layer components.[13]

The numbers of electrodes examined were 29 for 100 μm, 12 for 200 μm, and 10 for 300 μm. As portrayed in Fig. 4(a), data shown on ϕ_b–n graph come on the line (dashed line in the figure), meaning that the Schottky barrier height of the WC SBDs is largely homogeneous within a single diamond sample. An intrinsic Schottky barrier height ϕ_b°, which is obtained by extrapolating ϕ_b to n = 1 along the line, was 1.59 ± 0.02 eV, which is comparable to the value presented in an earlier report.[14] Considering ϕ_b°, N_A, and homoepitaxial layer thickness of the p^--type layer, the depletion layer expands within the entire p^--type layer at zero bias voltage, which means that the diamond SBD is punch-through type device.

Mean values of Schottky barrier height $\langle\phi_b\rangle$ and ideality factor $\langle n\rangle$ are presented in Table I. Actually, $\langle n\rangle$ of WC SBDs, approx. 1.2, is smaller than that of Au SBD, 1.4.[15]

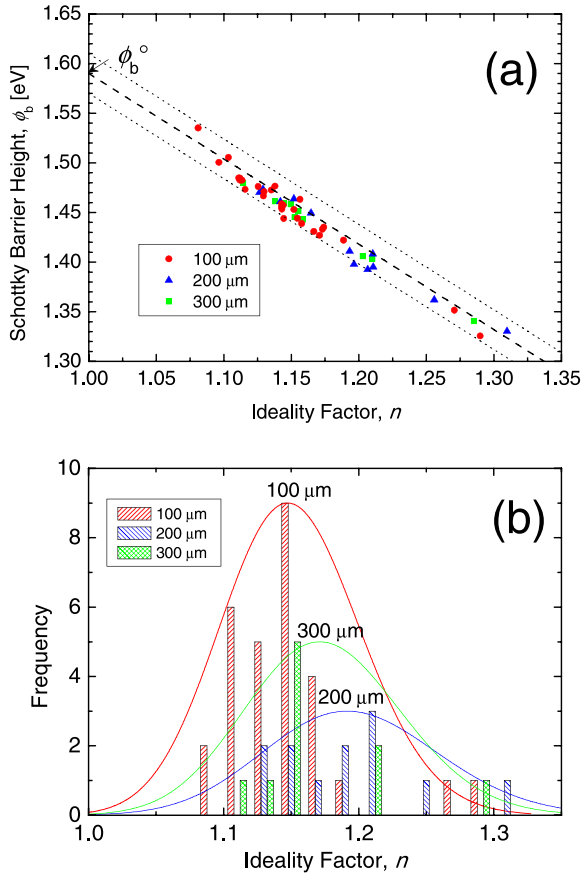

FIG. 4. (a) ϕ_b–n plot estimated from the forward characteristics of the whole electrode examined. (b) Distribution of ideality factor n at each electrode diameter.

Figure 4(b) shows correlation between n and the diameter of the Schottky electrode for 100–300 μm. Results show that $\langle n\rangle$ of 100 μm diameter was slightly smaller than that of larger diameter. A possible cause of the different n value is the less parallel conduction path for Schottky diodes for smaller diameter. This parallel conduction generally derives from traps and dislocations in the diamond crystal. If this is the case, then the areal number density of traps and dislocations is less than 3×10^3 cm^{-2} considering the critical diameter of 100 μm.

B. Reverse characteristics

As is true of the forward characteristics, the reverse current–density voltage (J_R–V) characteristics have no clear dependence on the electrode diameter. In this study, J_R–V characteristics of 300 μm were used for detailed analyses. Figure 5 shows typical J_R–V characteristic of the WC

TABLE I. Mean values of Schottky barrier height $\langle\phi_b\rangle$ and ideality factor $\langle n\rangle$.

	Schottky barrier height		Ideality factor	
Diameter (μm)	Mean value $\langle\phi_b\rangle$ (eV)	Standard deviation (eV)	Mean value $\langle n\rangle$	Standard deviation
100	1.46	0.04	1.15	0.04
200	1.42	0.05	1.19	0.05
300	1.43	0.04	1.17	0.05

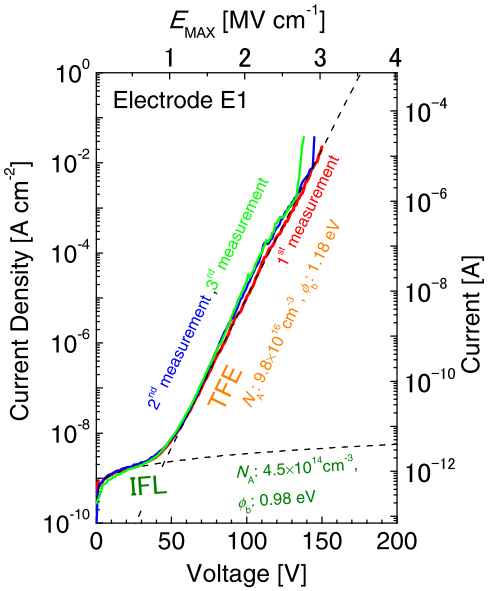

FIG. 5. Typical reverse *J*–*V* characteristics of the stable electrode E1, with a 300 μm diameter.

Schottky diodes. This electrode is designated as E1. The J_R–V characteristic changed its slope at the bias voltage of 40–70 V, which corresponds to the maximum electric field E_{max} of 0.8–1.4 MV cm^{-1}. In the case of silicon SBDs, the image-force lowering (IFL) of Schottky barrier height is a common mechanism of reverse current increase.[5] The reverse current density J_R including IFL effect is expressed as[5,6]

$$J_R = A^*T^2 \exp\left(\frac{-q\phi_b}{kT}\right)\exp\left(\frac{q\sqrt{qE_{max}/4\pi\varepsilon_D}}{kT}\right), \quad (2)$$

where ε_D is dielectric constant of diamond. Here, A^* of 90 A cm^{-2}K^{-2} and T of 300 K were used.

Results show that J_R of the electrode E1 can be fit well with the IFL model for lower reverse voltages of <40 V. Assuming that the ϕ_b of the electrode is spatially homogeneous, N_A and ϕ_b were inferred, respectively, from the fitting are 4.5×10^{14} cm^{-3} and 0.98 eV. The estimated N_A is smaller than the boron concentration derived from SIMS measurement: approx. 2×10^{15} cm^{-3}. However, ϕ_b of 0.98 eV is much lower than ϕ_b° of 1.6 eV or $\langle\phi_b\rangle$ of 1.4 eV, which are estimated from the J_F–V characteristics.

In the higher reverse voltage range above 60 V corresponding to >1.2 MV cm^{-1}, the reverse current increased exponentially until the current reached 2×10^{-5} A, which is the compliance current preset to the picoammeter/voltage source. The reverse bias voltage was applied to the SBDs up to 150 V, which corresponds to E_{max} of 3.0 MV cm^{-1}. This obtained E_{max} value is smaller than the highest values, reported as >7 MV cm^{-1},[2,16] but slightly larger than typical reported values to date of 2.1–2.3 MV cm^{-1}.[17,18] The J_R–V characteristic of this Schottky electrode changed slightly during repetition of the J_R–V measurements with the high electric field biasing.

The exponential increase of the reverse current is explained by the thermionic-field emission (TFE) model,[6] which has been observed frequently from SBDs fabricated using wide-gap semiconductors, such as SiC, GaN, and diamond.[3,11,19,20] Reverse current obeying the thermionic-field emission model is expressed as[3,6,11]

$$J_R = J_S \exp\left\{V\left(\frac{q}{kT} - \frac{1}{E_0}\right)\right\} \quad \text{and} \quad (3)$$

$$J_S = \frac{A^*T\sqrt{\pi qE_{00}}}{k}\left(q(V - V_P) + \frac{q\phi_b}{\cosh^2(qE_{00}/kT)}\right)^{1/2} \times \exp\left(\frac{-\phi_b}{E_0}\right), \quad (4)$$

where $E_0 = E_{00}\coth(E_{00}/kT)$, $E_{00} = h/4\pi\ [N_A/m^*\varepsilon_D]^{1/2}$, $V_P = E_F - E_V$, E_F stands for the Fermi level, E_V denotes the top of the valence band, and m^* represents the effective mass of electrons. Also, E_{00} is a parameter that reflects the carrier-tunneling probability.

The fitted curve is shown by the dashed line in Fig. 5. The N_A and ϕ_b are estimated using Eqs. (3) and (4) as 9.8×10^{16} cm^{-3} and 1.18 eV, respectively.

Results show that some Schottky electrodes exhibit a remarkable change of their J_R–V characteristics during the reverse bias operation. In other words, their reverse current level in the second measurement increased from that taken in the first measurement. Figure 6 shows the J_R–V characteristics of the electrode E2, for which the change was the most pronounced among the examined electrodes of 300 μm diameter. The fitting procedure is the same as that applied for electrode E1. In the lower voltage range below 40 V, N_A and ϕ_b of the electrode E2 were estimated, respectively, as 4.5×10^{14} cm^{-3} and 0.96 eV from the fitting by Eq. (2). Then, in the higher voltage range corresponding to the TFE mode, N_A of 7.2×10^{16} cm^{-3} and ϕ_b of 1.14 eV were obtained from Eqs. (3) and (4). These fitting parameters are comparable to those of the electrode E1, for which J_R–V

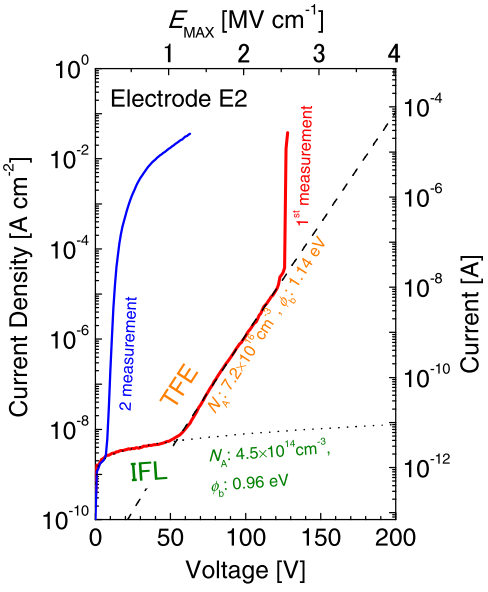

FIG. 6. Typical reverse *J*–*V* characteristic of the unstable electrode E2, with a 300 μm diameter.

characteristics changed slightly through high-voltage biasing. Therefore, except for this sudden current increase of electrode E2 at a higher voltage range, no marked difference was found in reverse characteristics between stable (E1) and unstable (E2) electrodes taken in the first measurement.

After this sudden current increase, the J_R–V characteristic of the unstable electrode E2 changed to a super-linear increase. For this study, 10 electrodes of 300 μm diameter were examined for the high reverse bias operation. Two caused a drastic and permanent change of the reverse current. It is noteworthy that some of the examined electrodes showed a sudden current increase in the first reverse characterization but did not increase their reverse current markedly in the second measurement. This fact implies that the deterioration mechanism involving the electric field breakdown is not so simple.

C. Origin of leakage current and electric field breakdown

To elucidate the cause of this sudden increase of the reverse current, the threshold reverse voltage V_{th} at which the reverse current reaches 10^{-7} A is shown as a function of ideality factor n of the electrode in Fig. 7(a). Data taken in the first measurements were used for this plot. No marked correlation was found between V_{th} (10^{-7} A) and n, meaning that V_{th} is difficult to deduce from the ideality factor derived from the forward characteristics. In most cases, V_{th} decreases rapidly with increasing electrode area because the probability that crystalline defects are located within one electrode becomes higher for the larger diameter electrodes.[21,22] Specific crystalline defects reportedly serve as a large leakage-current path.[23,24] In this study, V_{th} has moderate dependence on the electrode diameter, as portrayed in Fig. 7(b). Therefore, the sudden increase of reverse current is not caused by the crystalline defects in diamond. We understand that the diamond crystal examined in this study has markedly high quality that is suitable for evaluating reverse characteristics of SBDs.

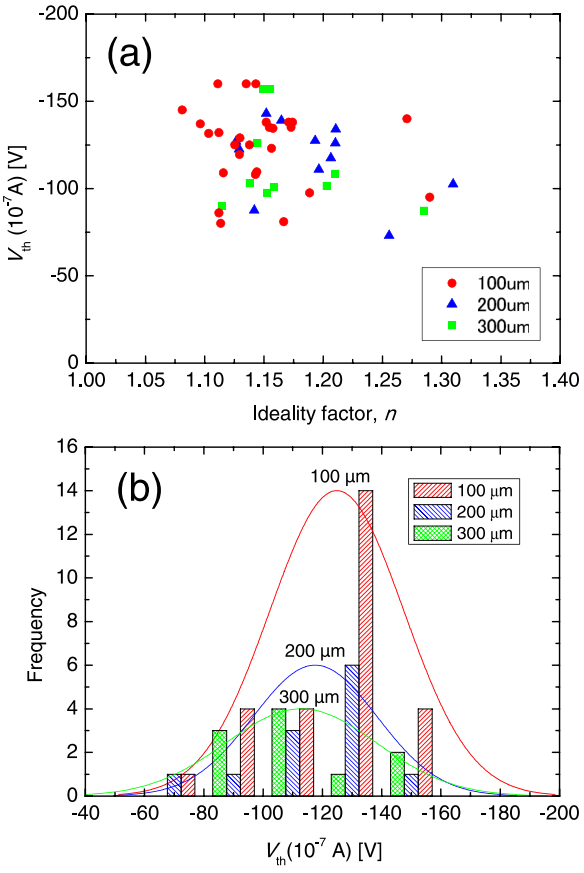

FIG. 7. (a) Reverse voltage at which the current reaches 10^{-7} A, V^{th}, in the first measurement as a function of n. (b) Distribution of V^{th} at each electrode diameter.

After the permanent change of the J_R–V characteristics, the J_F–V characteristics of the unstable electrodes E2 are changed slightly, as highlighted by green arrows in Fig. 8. A current subcomponent appeared as a shoulder at the forward voltage of approx. 0.5 V. The current component obtained using their subtraction is shown in the inset of Fig. 8. Results show that this subcomponent J_{sub}, which is the increased value of the forward current density through high reverse voltage biasing, can be fitted by the following equation:

$$J_{sub} = J_{s0} \exp\left(\frac{-qV}{n_{sub}kT}\right), \tag{5}$$

where J_{s0} is a constant and n_{sub} is an ideality factor of the subcomponents. n_{sub} was estimated as 2.1, indicating the current subcomponent is the recombination current.[5,6] For a lateral diode structure, recombination/generation current was observed from WC/p-diamond SBDs. The electrically active mid-gap states were thought to be formed near the diamond Schottky contact through the sudden current increase. Such a clear charge was rarely observed from other electrodes examined in this study, meaning that the forward characteristics are insensitive to the considerable change of reverse characteristics.

IV. DISCUSSION

A. Schottky barrier height inhomogeneity

ϕ_b° corresponds to the dominant Schottky barrier height within one electrode. n reflects the current transport mode

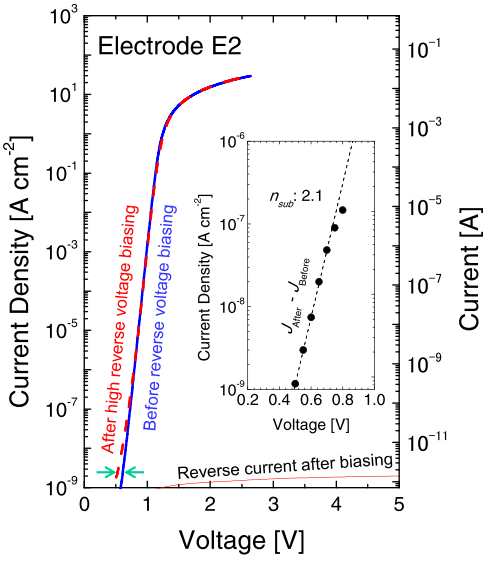

FIG. 8. Forward J–V characteristics of unstable electrodes before and after high-voltage biasing.

and spatial homogeneity of the Schottky barrier height. When *p*-diamond SBDs were fabricated using conventional process including wet-chemical oxidation treatment and selecting an inert metal such as Au for Schottky contact, the distribution width of ϕ_b° is greater than 0.2 eV.[3,15,25] In addition, the ϕ_b–*n* shown data of the conventional diamond SBDs have large dispersion, as represented by large *n* dispersion of ca. 0.1.

We have reported that the *n* dispersion of Au SBDs can be decreased to less than 0.05 by introducing the VUV/ozone oxidation treatment immediately before the Schottky metal deposition.[15,25] In the conventional SBD fabrication process, the annealing step that induces deterioration of oxygen termination is necessary for ohmic contact formation.[26] The main role of this treatment is to eliminate the annealing step from the SBD fabrication process.[15] Because the *p*-diamond samples with low-N_A of approx. 2×10^{15} cm^{-3} were used in these examinations, dominant current transport mode was the thermionic emission ($n = 1$). The decrease of *n* dispersion is understood to originate from improvement of spatial homogeneity of the Schottky barrier height using the VUV/ozone treatment. The distribution width of ϕ_b° decreased to less than 0.05 eV.

In this study, despite the use of the conventional process for WC SBD fabrication, the distribution width of ϕ_b° of 0.04 eV is equivalent to the case of Au SBDs fabricated using the VUV/ozone oxidation treatment. Neither an indentation mark nor breakage appeared on WC electrodes after multiple electrical measurements using tungsten microprobes, which contrasts greatly to easy scratching, peeling, or delamination of low-reactivity metal electrodes such as Au or Al.[15] This fact indicates that the WC Schottky contacts have better adhesion to the diamond surface than low-reactivity metal Schottky contacts do, in addition to the high mechanical hardness of the WC layer. WC/diamond Schottky contacts are regarded as having different interface structures from those of other low-reactivity metal Schottky contacts.

For Au SBDs prepared using VUV/ozone oxidation treatment, a key is to preserve oxygen termination even after the Schottky contact formation.[27] However, as evidenced by strong metal adhesion, chemical bonding is inferred to be formed at the WC/diamond interfaces during WC deposition. Apparently, most of the oxygen-terminated diamond surface is probably dissociated. Transmission electron microscopy revealed that the WC/diamond interface is abrupt in the nanometer-scale range and oxygen atoms are present near the interface.[28]

Considering these facts, the possible WC/diamond interface structure is understood as follows. Through WC deposition, most of the top-most carbon atoms of the diamond surface, which were originally terminated by oxygen groups before metal deposition, made chemical bonds with tungsten or carbon atoms constituting the WC layer. At the same time, terminated oxygen groups were dissociated from the diamond surface. Some top-most carbon atoms, which are distributed randomly near the interface, have a lone pair or keep oxygen termination. They are a possible origin that induces Schottky barrier height inhomogeneity at the WC/diamond interface. In our earlier report, the sputtered WC was known to be crystallized with small grains, although the grain size was not characterized yet.[10] The WC grain size might affect the Schottky barrier height homogeneity. These factors modify the ideality factor *n*. However, the small distribution width of ϕ_b° of 0.04 eV indicates that the interface homogeneity is markedly higher than similar data reported to date for diamond SBDs.

B. Reverse current at lower voltage range (<40 V)

Next, we discuss the reverse current transport mode at diamond Schottky contacts. In general, SBD is analyzed assuming the spatially uniform Schottky barrier height. Therefore, the metal/semiconductor interface will be described by a simple band diagram in the direction normal to the Schottky barrier interface. ϕ_b spatial variation within a circular electrode is shown schematically in Fig. 9(a). For TE mode current transport with spatially uniform ϕ_b, ϕ_b can be estimated easily using Eq. (1) with $n = 1$. Figure 9(b) presents an example of the band diagram near the metal/*p*-diamond interface under the reverse bias operation, where Schottky electrode metal is shown on the left-hand side whereas the valence band and the Fermi-level of the diamond are presented on the right-hand side.

Under a thermal equilibrium condition in which no external voltage is biased, the number of holes in the *p*-diamond with higher energy than the built-in potential V_{bi} is equal to that located in the metal with higher energy than ϕ_b. Because these higher-energy holes diffuse into mutually opposite sides, current that flows through the metal/*p*-diamond interface is macroscopically zero. When reverse bias V_R is applied to the Schottky diode, the energy barrier for the holes in *p*-diamond side becomes larger from V_{bi} to $V_{bi} + V_R$. Accordingly, hole injection from *p*-diamond to the Schottky metal becomes smaller with increasing V_R. Finally, hole injection from Schottky metal to *p*-diamond, as shown in Fig. 9(b), becomes a main component of the reverse current. This reverse current has little dependence on the external bias voltage because of the image force lowering (IFL) of the Schottky barrier.

As described earlier, the mean values of Schottky barrier height $\langle\phi_b\rangle$ obtained from the forward characteristics are approx. 1.45 eV, whereas ϕ_b estimated from the fitting of the reverse characteristic in the lower voltage region is approx. 1.0 eV. This discrepancy in estimated ϕ_b between forward and reverse characteristics is larger, although both the *J*–*V* characteristics fit the established model well. One possible cause that puts ϕ_b in a reverse bias condition lower is

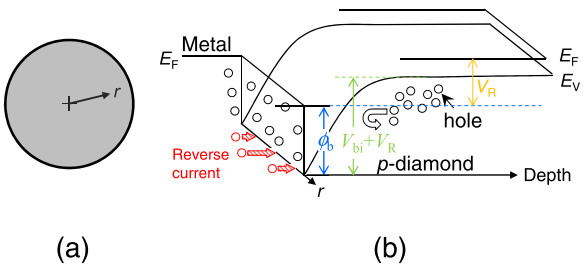

FIG. 9. (a) Distribution profile of spatially uniform Schottky barrier height within one electrode under the biasing condition of reverse voltage V_R and (b) corresponding band diagram near the metal–semiconductor interface.

inhomogeneous ϕ_b at the WC/*p*-diamond interface.[29,30] The low Schottky barrier height ϕ_b^{low} portion coexists in the patch shape in the ϕ_b° region, which forms dominantly within one electrode.

Figure 10(b) portrays a band diagram of WC/*p*-diamond in which the ϕ_b^{low} patch exists in one electrode. A reverse bias voltage is applied to the SBD. A schematic illustration of the non-uniform ϕ_b distribution is presented in Fig. 10(a), where two ϕ_b^{low} patches are depicted. The current transport mode in this diagram is thermionic-emission (TE) independent of ϕ_b because of the low N_A of approx. 2×10^{15} cm^{-3} of the *p*-diamond. The effect of localized ϕ_b^{low} patch on the current transport is substantial in the J_R–V characteristics, even if the area of ϕ_b^{low} patch is small, because the reverse current at Schottky contact flows dominantly through the ϕ_b^{low} patch, as indicated in Fig. 10(b). The reverse current raised by the ϕ_b^{low} patch is remarkable under lower reverse voltage V_R^{Low}, which corresponds to <40 V in this study. This ϕ_b^{low} patch does not affect the forward characteristics so much as in the case of reverse characteristics because the forward current in TE mode increases rapidly with bias voltage.

Because the ϕ_b^{low} area is much smaller than the entire electrode area, true ϕ_b^{low} is lower than the 1.0 eV estimated presuming the homogeneous barrier height within the electrode area. At this moment, the ϕ_b^{low} value remains uncertain because no suitable model is available to evaluate the ϕ_b^{low} area. Observation of the ϕ_b^{low} area using scanning internal photoemission microscopy[31] or electron-beam-induced current imaging[32] is expected to be powerful enough to evaluate the true ϕ_b^{low} value. The number of the ϕ_b^{low} patches and their area might correlate with the Schottky barrier height inhomogeneity discussed in Sec. IV A. Further investigation is necessary to elucidate the origin of ϕ_b^{low} patches and their formation mechanism.

C. Reverse current at higher voltage range (>60 V)

Following this TE transport mode with IFL, reverse current in TFE mode appeared in a higher reverse voltage range. The N_A of approx. 10^{17} cm^{-3} estimated from the transport analysis by TFE mode is more than a tenfold of the value obtained from the SIMS measurement. This overestimation of N_A might derive from an increase of the carrier tunneling probability. The tunneling probability is regarded as enhanced by the electric field concentration at the Schottky electrode fringe,[33] as presented in Fig. 11(a). When the electric field

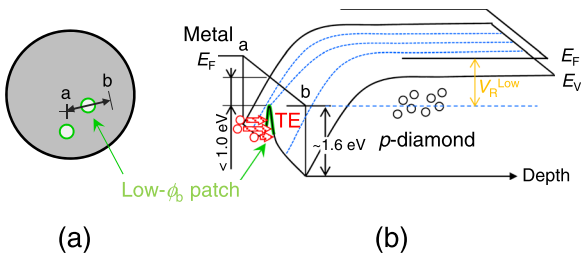

FIG. 10. (a) Distribution profile of spatially nonuniform Schottky barrier heights within one electrode under the biasing condition of reverse voltage V_R^{Low} of <40 V and (b) corresponding band diagram near the metal–semiconductor interface.

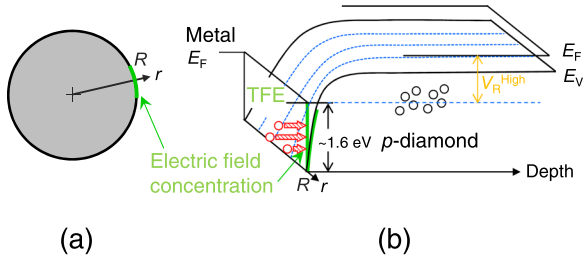

FIG. 11. (a) Distribution profile of Schottky barrier height with electric field concentration under the biasing condition of reverse voltage V_R^{High} of >60 V and (b) corresponding band diagram near the metal–semiconductor interface.

concentration occurred under the high reverse voltage biasing, the band bending became steeper locally, as portrayed in Fig. 11(b). The Schottky barrier height under the high electric field concentration condition, ϕ_b^{field}, is estimated as approx. 1.2 eV assuming TFE mode. Because ϕ_b decreases by IFL in TFE mode (e.g., 2 MV cm^{-1}) is 0.2 eV, $\langle\phi_b\rangle$ can be estimated from reverse characteristics to be 1.4 eV by adding ϕ_b^{field} of 1.2 eV and 0.2 eV of IFL. This value is consistent with $\langle\phi_b\rangle$ of approx 1.45, estimated from forward characteristics. The slope of J_R–V characteristics in this high voltage range is expected to decrease by the edge termination of the Schottky electrode.[5,6]

Relative to the sudden increase in current, no marked difference was found in the J_R–V characteristics between the stable (E1) and the unstable (E2) electrodes, as described previously. This fact suggests that the sudden increase in current is not caused by the degree of either ϕ_b^{low} patch or the electric field concentration. After the permanent change of the J_R–V characteristic, the reverse current is regarded as flowing dominantly through the defective area near the electrode fringe.

The electric field reportedly concentrates when an electrode has nanometer-scale thickness[34] which indicates that the field concentration factor is determined simply by the electrode film thickness. When assuming N_A of 9.8×10^{16} cm^{-3}, E_{max} at the electric-field-enhanced area is estimated as 4.4 MV cm^{-1} at reverse voltage of 150 V. This value is 1.4 times higher than the situation in which no electric-field enhancement occurs: 3 MV cm^{-1}. This value of electric field enhancement is lower than that of lateral SBD structure of 40.[3] In this study, the TFE transport region was clearly observed in a wide range of the J_R–V characteristic, compared to the case of other common semiconductors. This fact is attributable to the high breakdown field of diamond, highly stable WC Schottky electrodes, and lower leakage current level of SBD. From such a perspective, diamond is a suitable semiconductor material to investigate reverse current properties under high bias voltage.

V. CONCLUSION

We investigated the reverse current transport mode of tungsten carbide/*p*-diamond (100) Schottky contacts. Reverse current increased according to the thermionic emission mechanism with image force lowering of Schottky barrier in the lower voltage region, whereas the thermionic-field emission mode became dominant when the maximum electric field of the Schottky barrier diodes becomes larger

than 1 MV cm^{-1}. The Schottky barrier height estimated from reverse characteristics is lower than that from the forward characteristics. This discrepancy is interpreted by the spatially inhomogeneous Schottky barrier height. Current transport by the thermionic-field emission was found to be enhanced by the electric field concentration, presumably at the electrode fringe.

ACKNOWLEDGMENTS

The authors would like to thank Dr. M. Y. Liao, Dr. M. Imura, and Dr. Y. Garino of NIMS for helping with preparation of the sample and electrical measurements. We also would like to thank Dr. H. Umezawa of AIST for fruitful discussion. This work was partly supported by Grants-in-Aid for Scientific Research from the Ministry of Education, Culture, Sports, Science, and Technology, Japan (Grant Nos. 15H03980, 26220903, 16H06326, and 16H03861) and Cross-ministerial Strategic Innovation Promotion Program (SIP), "Next Generation Power Electronics" from Cabinet Office, Japan.

[1]J. E. Butler, M. W. Geis, K. E. Krohn, J. Lawless, Jr., S. Deneault, T. M. Lyszczarz, D. Flechtner, and R. Wright, Semicond. Sci. Technol. **18**, S67 (2003).
[2]P. N. Volpe, P. Muret, J. Pernot, F. Omnès, T. Teraji, Y. Koide, F. Jomard, D. Planson, P. Brosselard, N. Dheilly, B. Vergne, and S. Scharnholz, App. Phys. Lett. **97**, 223501 (2010).
[3]T. Teraji, S. Koizumi, Y. Koide, and T. Ito, Jpn. J. Appl. Phys., Part 2 **46**, L196 (2007).
[4]H. Umezawa, K. Ikeda, R. Kumaresan, N. Tatsumi, and S. Shikata, IEEE Electron Device Lett. **30**, 960 (2009).
[5]S. M. Sze, *Physics of Semiconductor Devices*, 2nd ed. (Wiley, New York, 1981).
[6]E. H. Rhoderick and R. H. Williams, *Metal–Semiconductor Contacts*, 2nd ed. (Oxford University Press, Oxford, 1988).
[7]M. Yokoba, Y. Koide, A. Otsuki, F. Ako, T. Oku, and M. Murakami, J. Appl. Phys. **81**, 6815 (1997).
[8]M. Liao, J. Alvarez, and Y. Koide, Jpn. J. Appl. Phys., Part 1 **44**, 7832 (2005).
[9]M. Y. Liao, Y. Koide, J. Alvarez, M. Imura, and J.-P. Kleider, Phys. Rev. B **78**, 045112 (2008).
[10]M. Y. Liao, Y. Koide, and J. Alvarez, J. Vac. Sci. Technol. B **24**, 185 (2006).
[11]H. Umezawa, T. Saito, N. Tokuda, M. Ogura, S. G. Ri, H. Yoshikawa, and S. Shikata, Appl. Phys. Lett. **90**, 073506 (2007).
[12]T. Teraji, M. Y. Liao, and Y. Koide, J. Appl. Phys. **111**, 104503 (2012).
[13]A. Fiori, T. Teraji, and Y. Koide, Phys. Status Solidi A **211**, 2363 (2014).
[14]A. Fiori, T. Teraji, and Y. Koide, Appl. Phys. Lett. **105**, 133515 (2014).
[15]T. Teraji, Y. Garino, Y. Koide, and T. Ito, J. Appl. Phys. **105**, 126109 (2009).
[16]A. Traoré, P. Muret, A. Fiori, D. Eon, E. Gheeraert, and J. Pernot, App. Phys. Lett. **104**, 052105 (2014).
[17]H. Umezawa, Y. Kato, and S. Shikata, Appl. Phys. Express **6**, 011302 (2013).
[18]M. Suzuki, T. Sakai, T. Makino, H. Kato, D. Takeuchi, M. Ogura, H. Okushi, and S. Yamasaki, Phys. Status Solidi A **210**, 2035 (2013).
[19]J. Suda, K. Yamaji, Y. Hayashi, T. Kimoto, K. Shimoyama, H. Namita, and S. Nagao, Appl. Phys. Express **3**, 101003 (2010).
[20]T. Hatakeyama and T. Shinohe, Mater. Sci. Forum **389–393**, 1169 (2002).
[21]H. Umezawa, K. Ikeda, N. Tatsumi, R. Kumaresan, and S. Shikata, Diamond Relat. Mater. **18**, 1196 (2009).
[22]H. Umezawa, Y. Mokuno, H. Yamada, A. Chayahara, and S. Shikata, Diamond Relat. Mater. **19**, 208 (2010).
[23]S. Ohmagari, T. Teraji, and Y. Koide, J. Appl. Phys. **110**, 056105 (2011).
[24]T. Shimaoka, T. Teraji, K. Watanabe, and S. Koizumi, Phys. Status Solidi A (in press).
[25]Y. Garino, T. Teraji, S. Koizumi, Y. Koide, and T. Ito, Phys. Status Solidi A **206**, 2082 (2009).
[26]T. Teraji, Y. Koide, and T. Ito, Thin Solid Films **557**, 241 (2014).
[27]T. Teraji, Y. Koide, and T. Ito, Phys. Status Solidi (r) **3**, 211 (2009).
[28]J. C. Piñero, D. Araújo, A. Fiori, A. Traoré, M. P. Villar, D. Eon, P. Muret, J. Pernot, and T. Teraji, Appl. Surf. Sci. **395**, 200 (2017).
[29]R. T. Tung, Mater. Sci. Eng. R **35**, 1 (2001).
[30]P. Muret, A. Traoré, A. Maréchal, D. Eon, J. Pernot, J. C. Piñero, M. P. Villar, and D. Araújo, J. Appl. Phys. **118**, 204505 (2015).
[31]K. Shiojima, S. Yamamoto, Y. Kihara, and T. Mishima, Appl. Phys. Express **8**, 046502 (2015).
[32]S. Kono, T. Teraji, H. Kodama, and A. Sawabe, Diamond Relat. Mater. **59**, 54 (2015).
[33]K. Ikeda, H. Umezawa, N. Tatsumi, K. Ramanujam, and S. Shikata, Diamond Relat. Mater. **18**, 292 (2009).
[34]H. Matsubara, Y. Saitoh, O. Maida, T. Teraji, K. Kobayashi, and T. Ito, Diamond Relat. Mater. **16**, 1044 (2007).